PHOTONICS Research

Floating terahertz metamaterials with extremely large refractive index sensitivities

Harry Miyosi Silalahi,[1] Yin-Pei Chen,[1] Yi-Hong Shih,[2] Yu-Shao Chen,[1] Xin-Yu Lin,[1] Jih-Hsin Liu,[3] and Chia-Yi Huang[1,*]

[1]Department of Applied Physics, Tunghai University, Taichung 40704, China
[2]Department of Photonics, Taiwan Cheng Kung University, Tainan 70101, China
[3]Department of Electrical Engineering, Tunghai University, Taichung 40704, China
*Corresponding author: chiayihuang@thu.edu.tw

Received 4 June 2021; revised 26 July 2021; accepted 9 August 2021; posted 10 August 2021 (Doc. ID 433335); published 15 September 2021

In the diagnosis of severe contagious diseases such as Ebola, severe acute respiratory syndrome, and COVID-19, there is an urgent need for protein sensors with large refractive index sensitivities. Current terahertz metamaterials cannot be used to develop such protein sensors due to their low refractive index sensitivities. A simple method is proposed that is compatible with all geometrical structures of terahertz metamaterials to increase their refractive index sensitivities. This method uses patterned photoresist to float the split-ring resonators (SRRs) of a terahertz metamaterial at a height of 30 μm from its substrate that is deposited with complementary SRRs. The floating terahertz metamaterial has an extremely large refractive index sensitivity of 532 GHz/RIU because its near field is not distributed over the substrate and also because the complementary SRRs confine the field above the substrate. The floating terahertz metamaterial senses bovine serum albumin (BSA) and the protein binding of BSA and anti-BSA as BSA, and anti-BSA solutions with low concentrations that are smaller than 0.150 μmol/L are sequentially dropped onto it. The floating terahertz metamaterial is a great achievement to develop protein sensors with extremely large refractive index sensitivities, and has the potential to sense dangerous viruses.

https://doi.org/10.1364/PRJ.433335

1. INTRODUCTION

Terahertz metamaterials, which comprise arrays of microscale split-ring resonators (SRRs), have been used to detect the dielectric materials that are deposited on them because the resonance frequencies of the metamaterials are sensitive to the effective refractive indices n_{eff} of the combined contribution of their substrates and the dielectric materials [1–4]. n_{eff} equals $\eta\,[\chi n_{\text{sub}} + (1-\chi)n_{\text{die}}]$, where η is a geometrical factor of the SRRs of a terahertz metamaterial; χ $(0 \le \chi \le 1)$ is a weight factor of the contribution of its substrate to n_{eff}; n_{sub} refers to the refractive index of the substrate; and n_{die} is the refractive index of the dielectric material deposited on the metamaterial [5]. The key performance parameter for a terahertz metamaterial is to have a large refractive index sensitivity S. S is defined as the ratio of the shifting range Δf of the resonance frequencies of the terahertz metamaterial to a change Δn in the refractive indices of the two dielectric materials that are deposited on it separately [6,7]. Δf is proportional to a change Δn_{eff} in the effective refractive indices of the substrate and dielectric materials [5]. Therefore, S will increase significantly when Δn_{eff} is large enough.

Previous works used terahertz metamaterials in which each of their SRRs had a single gap to sense dielectric materials, and the refractive index sensitivities of the metamaterials were smaller than 200 GHz/RIU [8–10]. The refractive index sensitivities of terahertz metamaterials are increased to 300 GHz/RIU using SRRs with multigaps because they interact more with the dielectric materials that are deposited on them [11–13]. The near fields of the terahertz metamaterials that involve the single gaps and multigaps are distributed over their substrates and dielectric materials because the terahertz metamaterials are deposited on the substrates [14,15]. These fields sense small changes in $\Delta n_{\text{eff}} = \eta \times (1-\chi) \times \Delta n$ due to $\chi \neq 0$. Therefore, the terahertz metamaterials that involve the single gaps and multigaps have limited refractive index sensitivities. This drawback hinders the usage of these metamaterials in sensing microorganisms such as bacteria and viruses. If the near fields of terahertz metamaterials are all in the dielectric materials that are deposited on them ($\chi = 0$), the fields will more strongly interact with the dielectric materials. Therefore, the terahertz metamaterials have large frequency shifting ranges due to $\Delta n_{\text{eff}} = \eta \Delta n$.

This work fabricates floating terahertz metamaterials by lifting the SRRs of terahertz metamaterials at various floating heights from their substrates that are deposited with complementary SRRs using photoresist patterns. Experimental results reveal that the floating terahertz metamaterial at a height of 30 μm has an extremely large refractive index sensitivity of 532 GHz/RIU, which exceeds those of the previous terahertz metamaterials [8–12]. Simulated results reveal that the photoresist patterns and complementary SRRs cause the near field of the floating terahertz metamaterial not to be in its substrate ($\chi = 0$). Therefore, the floating of the terahertz metamaterial significantly increases its refractive index sensitivity. The floating terahertz metamaterial senses bovine serum albumin (BSA) and the protein binding of BSA and anti-BSA as BSA, and anti-BSA solutions with low concentrations that are smaller than 0.150 μmol/L are sequentially dropped onto it. The BSA solution has a lower concentration in this work than in the previous work [11]. This floating terahertz metamaterial can be used to detect proteins such as antigens and antibodies, and has the potential to sense dangerous viruses such as Ebola, severe acute respiratory syndrome (SARS), and COVID-19. This work proposes a simple method to increase the refractive index sensitivities of metamaterials by floating them using photoresist patterns, and the method is compatible with all geometrical structures of metamaterials such as fishnets, rods, and dots.

2. MATERIALS AND METHODS

Figure 1(a) presents the schematic drawing of floating terahertz metamaterials. Photoresist patterns (SU-8 3010, Kayaku Advanced Materials (formerly MicroChem Corp.), Newton, MA, USA) are deposited on a glass substrate using photolithography. A silver film with a thickness of 200 nm is coated on the photoresist patterns and substrate using a thermal evaporator. A floating terahertz metamaterial with an area of 1.0 cm × 1.0 cm is obtained following the evaporation. In brief, each of the floating terahertz metamaterials comprises SRRs, photoresist patterns, and complementary SRRs. Each of the SRRs of the floating terahertz metamaterials has a linewidth (w), gap (g), short side (s), long side (l), a period in the x direction, and a period in the y direction of 6 μm, 20 μm, 50 μm, 60 μm, 70 μm, and 80 μm, respectively. The floating terahertz metamaterials have the photoresist patterns with various heights (h) of 6.6 μm, 13.4 μm, 18.2 μm, 27.2 μm, and 30 μm.

Figure 1(b) presents the schematic drawing of a common terahertz metamaterial. Silver SRRs are deposited on a glass substrate using photolithography, evaporation, and a lift-off process. The common terahertz metamaterial is obtained following the lift-off process. The SRRs in the common terahertz metamaterial have the same configuration and geometrical dimensions as those in the floating terahertz metamaterials.

Figures 1(c) and 1(d) present the schematic drawing of the fluid cells with the floating and common terahertz metamaterial, respectively. Two polycarbonate spacers with a thickness of 200 μm are placed at the two sides of each of the glass substrates with the floating and common terahertz metamaterials. A polyethylene terephthalate (PET) substrate with a thickness of 188 μm is placed on the spacers. Each empty cell comprises a glass substrate with one of the floating and common terahertz metamaterials and a PET substrate. The empty cells are filled with air or glycerol. The fluid cells with the floating and common terahertz metamaterials are obtained following the filling.

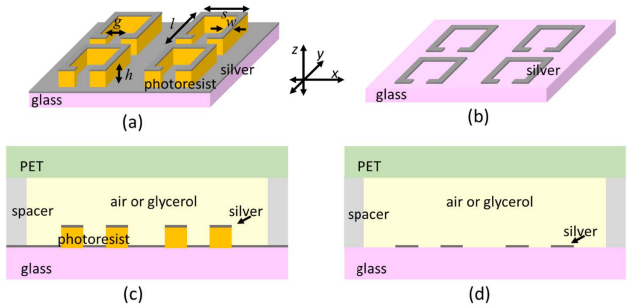

Fig. 1. Schematic drawing of (a) floating terahertz metamaterials and (b) common terahertz metamaterial. Schematic drawing of fluid cells with (c) floating terahertz metamaterials and (d) common terahertz metamaterial.

3. RESULT AND DISCUSSION

A. Floating and Common Terahertz Metamaterials

Figure 2(a) presents the experimental spectra of the floating terahertz metamaterial with the air and glycerol overlayers at $h = 30$ μm. The spectra are measured with a terahertz spectrometer (TPS 3000, TeraView) in transmission mode, and the polarized direction of incident terahertz waves is set parallel to the gaps of the SRRs shown in Fig. 1(a). The incident terahertz waves have a beam diameter of 6 mm in this work, and a frequency resolution of 3 GHz is used in the spectral measurement. The chamber in the spectrometer is filled with nitrogen gas to prevent terahertz waves from absorbing water vapor. The spectrum of the nitrogen gas as a reference signal is used to normalize those of the fluid cells. Glycerol (air) has a refractive index n_{gly} (n_{air}) of 1.47 (1.0) in the terahertz region, and was

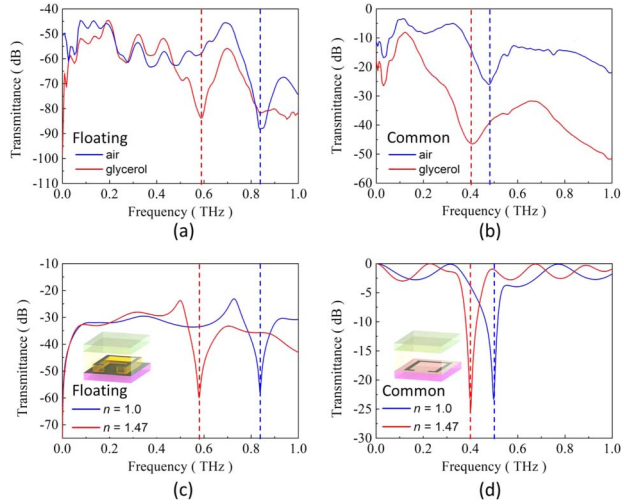

Fig. 2. (a) Experimental and (c) simulated spectra of floating terahertz metamaterial with air and glycerol overlayers at $h = 30$ μm. (b) Experimental and (d) simulated spectra of common terahertz metamaterial with air and glycerol overlayers.

obtained from its time-domain spectrum. The resonance frequency (0.59 THz) of the floating terahertz metamaterial with the glycerol overlayer is red shifted from that (0.84 THz) of the floating terahertz metamaterial with the air overlayer due to a difference between n_{air} and n_{gly}. The floating terahertz metamaterial at $h = 30$ μm exhibits a frequency shifting range of 250 GHz, so it has a refractive index sensitivity of 532 (= 250/0.47) GHz/RIU. This metamaterial has a larger refractive index sensitivity than previous metamaterials [8–12]. This result is a great achievement for the development of terahertz metamaterials with extremely large refractive index sensitivities.

Figure 2(b) presents the experimental spectra of the common terahertz metamaterial with the air and glycerol overlayers. The resonance frequency (0.40 THz) of the common terahertz metamaterial with the glycerol overlayer is red shifted from that (0.48 THz) of the common terahertz metamaterial with the air overlayer. The common terahertz metamaterial exhibits a frequency shifting range of 80 GHz, so it has a refractive index sensitivity of 170 (= 80/0.47) GHz/RIU. Therefore, the floating terahertz metamaterial at $h = 30$ μm has a refractive index sensitivity three times that of the common terahertz metamaterial.

Hu *et al.* reported that the metamaterial integrated with the microfluidic channel has an experimental sensitivity of 3.5 THz/RIU at the illumination of obliquely incident terahertz beams [16]. Therefore, this metamaterial is a reflective sensor with high performance. Yan *et al.* used the graphene-based grating integrated with the Fabry–Perot cavity to a reflective sensor [17]. The reflective sensor has a simulated sensitivity of 4.2 THz/RIU, so the graphene-based grating integrated with the Fabry–Perot cavity has the potential in biochemical sensing. Reflective sensors are difficult to integrate terahertz sources and detectors into single and compact devices due to the oblique incidence and reflection of terahertz beams. Liang *et al.* used the grating integrated with the microfluidic channel to develop a transmissive sensor for detecting dielectric materials [18]. The transmissive sensor has a simulated sensitivity of 0.38 THz/RIU. However, the grating integrated with the microfluidic channel is difficult to fabricate because its Fabry–Perot resonance is very sensitive to the channel thickness. The difficult fabrication hinders the practical application of the transmissive sensor. Our work uses the floating metamaterial to develop a transmissive sensor with an experimental sensitivity of 0.532 THz/RIU. The floating metamaterial is easy to fabricate, and the proposed method is compatible with all geometrical structures of metamaterials.

The refractive index sensitivities S of metamaterials are not comparable at different operation frequency bands because the frequency shifting range of a metamaterial is usually smaller at a low operation frequency band than at a high operation frequency band. Normalized refractive index sensitivities S_N of metamaterials can be used to evaluate their performance at different operation frequency bands. The normalized refractive index sensitivity of a metamaterial is given by $S_N = S/f_{min}$, where f_{min} is the minimum resonance frequency in its operation frequency band [19]. Lan *et al.* reported that the metamaterial integrated with the microfluidic channel has a simulated S_N of 0.51/RIU [19]. The floating metamaterial has an S_N of 0.90/RIU in our work because its experimental S and f_{min} are 0.532 THz/RIU and 0.59 THz, respectively. Therefore, the floating metamaterial has a larger normalized refractive index sensitivity than the metamaterial integrated with the microfluidic channel.

A simulation is performed using Lumerical software to verify the simulated resonance spectra of the floating and common terahertz metamaterials with the air and glycerol overlayers. Two unit cells are used in the simulation, as presented in the insets of Figs. 2(c) and 2(d). The unit cells in the insets of Figs. 2(c) and 2(d) have the same geometrical structures as in Figs. 1(c) and 1(d). The glass substrates, PET substrates, and photoresist pattern in the unit cells have refractive indices of 2.25 [20], 1.73 [21], and 1.65 [22], respectively. The silver films in the unit cells have a conductivity of 6.30×10^7 S/m. A dielectric overlayer with a thickness of 200 μm in each of the unit cells has a refractive index of n, and n equals 1.0 (1.47) for air (glycerol). A periodical boundary condition is used in the simulation.

Figure 2(c) presents the simulated spectra of the floating terahertz metamaterial with the air and glycerol overlayers at $h = 30$ μm. The simulated resonance frequency (0.577 THz) of the floating terahertz metamaterial with the glycerol overlayer is red shifted from that (0.829 THz) of the floating terahertz metamaterial with the air overlayer. The floating terahertz metamaterial at $h = 30$ μm exhibits a simulated frequency shifting range of 252 GHz, so it has a simulated refractive index sensitivity of 536 (= 252/0.47) GHz/RIU.

Figure 2(d) presents the simulated spectra of the common metamaterial with the air and glycerol overlayers. The simulated resonance frequency (0.401 THz) of the common metamaterial with the glycerol overlayer is red shifted from that (0.489 THz) of the common metamaterial with the air overlayer. The common metamaterial exhibits a simulated frequency shifting range of 88 GHz, and it has a simulated refractive index sensitivity of 187 (= 88/0.47) GHz/RIU. The simulation spectra of Figs. 2(c) and 2(d) verify the experimental spectra of Figs. 2(a) and 2(b). The fluid cells have smaller (larger) experimental resonance transmittances (bandwidths) than simulated ones because the imaginary parts of the refractive indices of glass, photoresist, dielectric materials, and PET are not considered in the simulation of the fluid cells. The unexpected fluctuation of the experimental spectra in Figs. 2(a) and 2(b) arises from the multiple reflections of the fluid cells [23].

Figures 3(a) and 3(b) present the near-field distribution of one of the SRRs in the common (floating) metamaterial with the glycerol overlayer. The top views in Figs. 3(a) and 3(b) reveal that the floating SRR has a larger hot spot than the common SRR. Therefore, the floating SRR has a stronger near field than the common SRR. In other words, the floating SRR interacts more with the glycerol layer than the common SRR. This result shows that the floating SRR is highly sensitive to dielectric overlayers. The side views in Figs. 3(a) and 3(b) reveal that the near field of the floating SRR is distributed over the glycerol overlayer and photoresist pattern, but that of the common SRR is distributed over the glycerol overlayer and glass substrate. The near field of the floating SRR is not

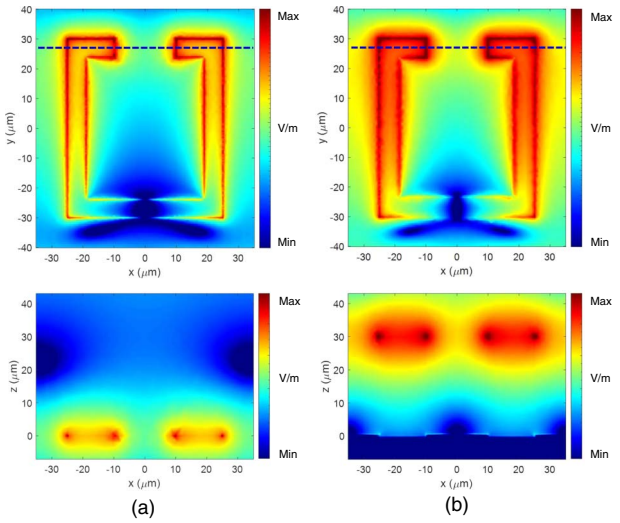

Fig. 3. Near-field distributions of SRRs of (a) common and (b) floating terahertz metamaterials with glycerol overlayers.

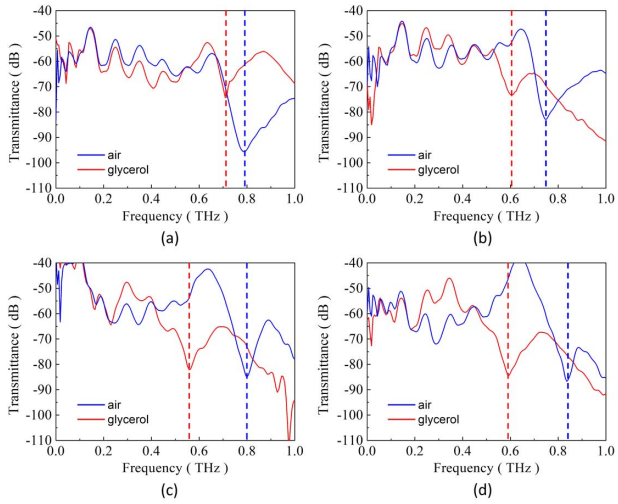

Fig. 5. Experimental spectra of floating terahertz metamaterials with air and glycerol overlayers at h of (a) 6.6 μm, (b) 13.4 μm, (c) 18.2 μm, and (d) 27.2 μm.

distributed over the glass substrate, and the complementary SRR confines the field above the substrate. Therefore, the floating SRR does not sense the glass substrate. In other words, the refractive index of the glass substrate does not contribute to the resonance frequency of the floating SRR.

B. Heights of Photoresist Patterns

The experimental results in Fig. 2(a) depict that as the photoresist patterns have a height of 30 μm, the floating metamaterial has an extremely large refractive index sensitivity of 532 GHz/RIU. Therefore, it is interesting to study the effect of the heights (h) of photoresist patterns on the refractive index sensitivities of floating metamaterials. Figures 4(a)–4(d) present the SEM images of the floating metamaterials with the photoresist patterns at $h = 6.6$ μm, 13.4 μm, 18.2 μm, and 27.2 μm, respectively.

Figures 5(a)–5(d) present the experimental spectra of the floating terahertz metamaterials with the air and glycerol overlayers at $h = 6.6$ μm, 13.4 μm, 18.2 μm, and 27.2 μm, respectively. The floating terahertz metamaterials have frequency shifting ranges of 70 GHz, 150 GHz, 243 GHz, and 246 GHz at $h = 6.6$ μm, 13.4 μm, 18.2 μm, and 27.2 μm, respectively. The frequency shifting ranges increase with an increase in the heights of the photoresist patterns. In addition, the floating terahertz metamaterials have the same difference between the refractive indices of air and glycerol. Therefore, the heights of the photoresist patterns increase the refractive index sensitivities of the floating terahertz metamaterials. This result reveals that the refractive index sensitivity of a floating terahertz metamaterial can be tuned by changing the height of its photoresist patterns.

Figures 6(a)–6(d) present the near-field distributions of the SRRs of the floating terahertz metamaterials with the glycerol overlayers at $h = 6.6$ μm, 13.4 μm, 18.2 μm, and 27.2 μm, respectively. As h is at 6.6 μm, the near field of the floating SRR is distributed over the glycerol overlayer, photoresist

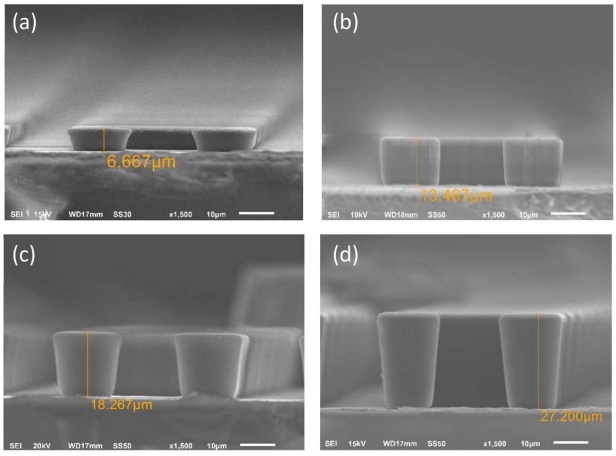

Fig. 4. SEM images of floating terahertz metamaterials with photoresist patterns at h of (a) 6.6 μm, (b) 13.4 μm, (c) 18.2 μm, and (d) 27.2 μm.

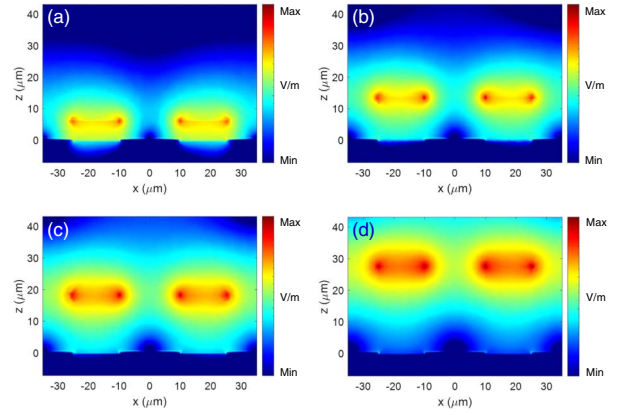

Fig. 6. Near-field distributions of SRRs of floating terahertz metamaterials with glycerol overlayers at h of (a) 6.6 μm, (b)13.4 μm, (c) 18.2 μm, and (d) 27.2 μm.

pattern, and glass substrate. The weight factor of the glass substrate to the effective refractive index of the media that surround this SRR exceeds zero because part of this field is in the glass substrate. Therefore, the floating terahertz metamaterial has a small frequency shifting range of 70 GHz at $h = 6.6$ μm. As h is increased to 13.4 μm, the weight factor of the glass substrate to the effective refractive index of the media that surround the floating SRR approaches zero since its near field is mainly distributed over the glycerol overlayer and photoresist pattern. Therefore, the floating terahertz metamaterial has a larger frequency shifting range at $h = 13.4$ μm than at $h = 6.6$ μm. As h exceeds 13.4 μm, the weight factor of the glass substrate to the effective refractive index of the media that surround the floating SRR equals zero because its near field is not distributed over the glass substrate. Therefore, the floating terahertz metamaterials have large frequency shifting ranges of 243 GHz and 246 GHz at $h = 18.2$ μm and 27.2 μm, respectively.

Figure 7 presents the experimental and simulated refractive index sensitivities of the floating terahertz metamaterials with the air and glycerol overlayers at $h = 6.6$ μm, 13.4 μm, 18.2 μm, 27.2 μm, and 30.0 μm. The floating terahertz metamaterials have experimental refractive index sensitivities of 149 GHz/RIU, 319 GHz/RIU, 517 GHz/RIU, 523 GHz/RIU, and 532 GHz/RIU at $h = 6.6$ μm, 13.4 μm, 18.2 μm, 27.2 μm, and 30.0 μm, respectively. These sensitivities approach a saturation value at an increase in h because the near fields [Figs. 6(a)–6(d)] of the floating terahertz metamaterials gradually weaken in the glass substrates. A simulation is performed to verify the effect of the heights of the photoresist patterns on the experimental refractive index sensitivities of the floating terahertz metamaterials. The experimental and simulated refractive index sensitivities have the same tendency to approach saturation values as h increases from 6.6 μm to 30.0 μm. The differences between the experimental and simulated refractive index sensitivities arise from imperfection of the fabrication of the floating terahertz metamaterials in Figs. 4(a)–4(d).

C. Application of Floating Terahertz Metamaterials

This section presents the capability of floating and common terahertz metamaterials to measure bovine serum albumin (BSA) and protein binding of BSA and anti-BSA. Figures 8(a) and 8(b) display the schematic drawings of the protein binding of BSA and anti-BSA on the floating and common terahertz metamaterials. The floating terahertz metamaterial has the same geometrical structures as the design of Fig. 1(a), but it is deposited on a PET substrate. The photoresist patterns in this metamaterial have a height of 30 μm. The common terahertz metamaterial has the same geometrical structures as the design of Fig. 1(b), but it is deposited on a PET substrate.

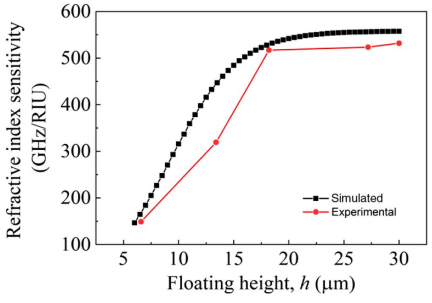

Fig. 7. Experimental and simulated refractive index sensitivities of floating terahertz metamaterials with air and glycerol overlayers at various floating heights.

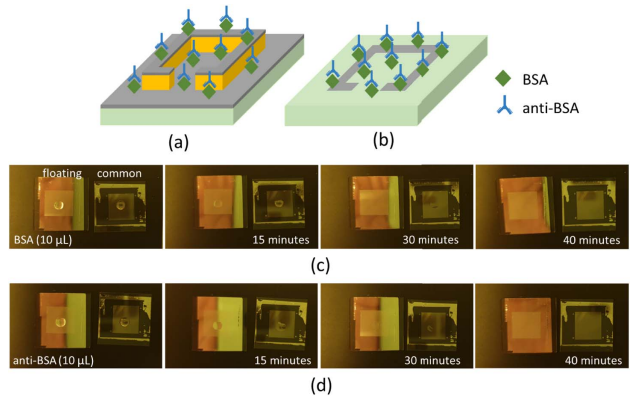

Fig. 8. Schematic drawings of protein binding of BSA and anti-BSA on (a) floating and (b) common terahertz metamaterials. Photos of water evaporation of (c) BSA and (d) anti-BSA aqueous solutions that are dropped on floating and common terahertz metamaterials.

A 10 μL BSA aqueous solution with a concentration of 0.110 μmol/L is dropped onto each of the floating and common terahertz metamaterials. The BSA aqueous solutions have a lower concentration in this work than in the previous work [11]. The floating and common terahertz metamaterials are placed in air at 25°C. The BSA layers are obtained after the BSA aqueous solutions completely dry on the floating and common terahertz metamaterials. The spectra of the floating and common terahertz metamaterials with the BSA layers are measured using the terahertz spectrometer.

A 10 μL anti-BSA aqueous solution with a concentration of 0.150 μmol/L is dropped onto each of the floating and common terahertz metamaterials with the BSA layers to observe the protein binding of anti-BSA and BSA. The floating and common terahertz metamaterials are placed in air at 25°C. The BSA/anti-BSA layers are obtained after the anti-BSA aqueous solutions completely dry on the floating and common terahertz metamaterials with the BSA layers. The floating and common terahertz metamaterials are washed with deionized water to remove unbound anti-BSA molecules, and are blown dry by nitrogen gas. The spectra of these metamaterials are measured using the terahertz spectrometer.

Figure 8(c) presents the photos of the water evaporation of the BSA aqueous solutions that are dropped on the floating and common terahertz metamaterials. The time for the water evaporation of the BSA aqueous solution is 30 (40) min for the floating (common) terahertz metamaterial as the water in the BSA solution completely dries. The BSA aqueous solution has a faster evaporation time on the floating terahertz metamaterial than on the common terahertz metamaterial because the former has a larger surface area than the latter.

Figure 8(d) presents the photos of the water evaporation of the anti-BSA aqueous solutions that are dropped on the floating and common terahertz metamaterials with the BSA layers. The time for the water evaporation of the anti-BSA aqueous solution is 30 (40) min on the floating (common) terahertz metamaterial with the BSA layers as the water in the anti-BSA solution completely dries. The sum of the evaporation times of the BSA and anti-BSA solutions is 60 (80) min for the floating (common) terahertz metamaterial. Therefore, the floating terahertz metamaterial has a faster response time to detect BSA and the protein binding of BSA and anti-BSA than the common terahertz metamaterial.

Figure 9(a) presents the experimental spectra of the floating terahertz metamaterial at the air overlayer, BSA layer, and BSA/anti-BSA layer. The floating terahertz metamaterial has resonance frequencies of 0.818 THz, 0.806 THz, and 0.800 THz at the air overlayer, BSA layer, and BSA/anti-BSA layer, respectively. This result reveals that the floating terahertz metamaterial experiences large differences between the effective refractive indices of the media that surround it. Therefore, the floating terahertz metamaterial distinguishes air, BSA, and BSA/anti-BSA as the BSA and anti-BSA solutions with low concentrations smaller than 0.150 μmol/L are sequentially dropped onto it. In other words, the floating terahertz metamaterial can sense dielectric materials with similar refractive indices.

Figure 9(b) presents the experimental spectra of the common terahertz metamaterial at the air overlayer, BSA layer, and BSA/anti-BSA layer. The common terahertz metamaterial has an identical resonance frequency of 0.479 THz at the air overlayer, BSA layer, and BSA/anti-BSA layer. This result reveals that the common terahertz metamaterial experiences tiny differences between the effective refractive indices of the media that surround it. Therefore, the common terahertz metamaterial does not distinguish air, BSA, and BSA/anti-BSA as the BSA and anti-BSA solutions with low concentrations smaller than 0.150 μmol/L are sequentially dropped onto it. In other words, the common terahertz metamaterial does not sense dielectric materials with similar refractive indices. The results in Figs. 9(a) and 9(b) show that the floating terahertz metamaterial can be used to develop protein sensors with fast response and extremely large refractive index sensitivities, and it has the potential to detect dangerous viruses such as Ebola, SARS, and COVID-19.

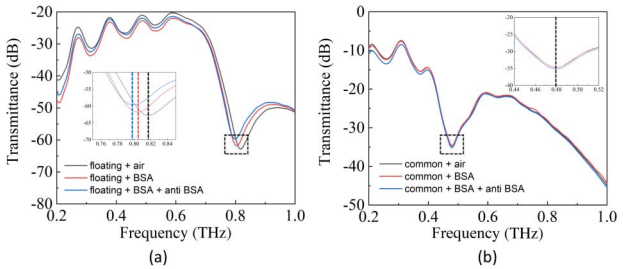

Fig. 9. (a) Experimental spectra of floating terahertz metamaterial at air overlayer, BSA layer, and BSA/anti-BSA layer. (b) Experimental spectra of common terahertz metamaterial at air overlayer, BSA layer, and BSA/anti-BSA layer.

The floating metamaterial cannot measure aqueous solutions in real-time due to the strong attenuation of terahertz waves in water vapor (data not shown herein). Therefore, the dried BSA layer and BSA/anti-BSA layers are detected in this work. Efforts are being made at the authors' laboratory to measure aqueous solutions using terahertz metamaterials, the results of which will be published in the near future.

4. CONCLUSION

New design, fabrication, simulation, characterization, and application of the floating terahertz metamaterials are proposed in this work. The common terahertz metamaterial is fabricated to evaluate the refractive index sensitivities of the floating terahertz metamaterials. The floating terahertz metamaterial has an extremely large refractive index sensitivity of 532 GHz/RIU at a floating height of 30 μm, but the common terahertz metamaterial has a small refractive index sensitivity of 170 GHz/RIU. The photoresist patterns and complementary SRRs cause the near field of the floating terahertz metamaterial not to be distributed over its substrate, so its refractive index sensitivity is three times that of the common terahertz metamaterial. The floating terahertz metamaterial detects BSA and the protein binding of BSA and anti-BSA as the BSA and anti-BSA solutions with low concentrations smaller than 0.150 μmol/L are sequentially dropped onto it, but the common terahertz metamaterial does not detect BSA and protein binding of BSA and anti-BSA in such solutions. We believe the floating terahertz metamaterial is a great achievement for sensing proteins such as antigens and antibodies, and has the potential to detect dangerous viruses such as Ebola, SARS, and COVID-19. This work proposes a simple method to increase the refractive index sensitivities of metamaterials by floating them via photoresist patterns, and the method is compatible with all geometrical structures of metamaterials such as fishnets, rods, and dots.

APPENDIX A: THEORETICAL ANALYSIS OF FLOATING METAMATERIAL

A theoretical analysis is used to explain that the floating terahertz metamaterial has a larger refractive index sensitivity than the common terahertz metamaterial. An SRR can be considered as an inductor-capacitor (LC) circuit, and its resonance frequency is given by [5]

$$f = \frac{1}{2\pi\sqrt{LC}} = \frac{c}{2\pi}\sqrt{\frac{g}{s \cdot l \cdot w}} \times \frac{1}{n_{\text{eff}}} = \frac{k}{n_{\text{eff}}}, \tag{A1}$$

where L is inductance of the inductor, and C is capacitance of the capacitor. L is determined by the enclosed area of the SRR, and C is proportional to an effective refractive index n_{eff} of the media that surround the SRR. s, l, w, and g in Eq. (A1) are defined in Fig. 1(a).

Consider that a common SRR is deposited on a glass substrate with a refractive index of n_{gla}, and is deposited with a dielectric overlayer with a refractive index of n_{die}. An effective refractive index $n_{\text{eff\_}C}$ of the media that surround the common SRR can be written as [5]

$$n_{\text{eff\_}C} = \eta[\alpha n_{\text{gla}} + (1-\alpha)n_{\text{die}}], \tag{A2}$$

where η is a geometrical factor of the common SRR, and α is a weight factor of the contribution of the glass substrate to $n_{\mathrm{eff\_}C}$. Substituting Eq. (A2) into Eq. (A1) yields a resonance frequency f_C of the common SRR, and f_C is given by

$$f_C = \frac{k}{\eta}\left[\frac{1}{\alpha n_{\mathrm{gla}} + (1-\alpha) n_{\mathrm{die}}}\right]. \tag{A3}$$

As the dielectric overlayer is changed from air with a refractive index of n_{air} to glycerol with a refractive index of n_{gly}, a frequency shifting range Δf_C of the common SRR can be expressed as

$$\Delta f_C = \frac{k}{\eta} \times \frac{n_{\mathrm{air}} - n_{\mathrm{gly}}}{\left(\frac{\alpha}{1-\alpha} n_{\mathrm{gla}} + n_{\mathrm{air}}\right)\left(\frac{\alpha}{1-\alpha} n_{\mathrm{gla}} + n_{\mathrm{gly}}\right)}. \tag{A4}$$

Consider that a floating SRR is lifted at a floating height of 30 μm from a glass substrate that is deposited with a complementary SRR using a photoresist pattern with a refractive index of n_{pho}, and is deposited with a dielectric overlayer with a refractive index of n_{die}. An effective refractive index $n_{\mathrm{eff\_}F}$ of the media that surround the floating SRR can be written as [5]

$$n_{\mathrm{eff\_}F} = \eta[\beta n_{\mathrm{pho}} + (1-\beta) n_{\mathrm{die}}], \tag{A5}$$

where η is a geometrical factor of the floating SRR, and β is a weight factor of the contribution of the photoresist pattern to $n_{\mathrm{eff\_}F}$. Because the floating and common SRRs have the same geometrical structure, they have the same geometrical factor. Substituting Eq. (A5) into Eq. (A1) yields a resonance frequency f_F of the floating SRR, and f_F is given by

$$f_F = \frac{k}{\eta}\left[\frac{1}{\beta n_{\mathrm{gla}} + (1-\beta) n_{\mathrm{die}}}\right]. \tag{A6}$$

As the dielectric overlayer is changed from air to glycerol, a frequency shifting range Δf_F of the floating SRR can be expressed as

$$\Delta f_F = \frac{k}{\eta} \times \frac{n_{\mathrm{air}} - n_{\mathrm{gly}}}{\left(\frac{\beta}{1-\beta} n_{\mathrm{pho}} + n_{\mathrm{air}}\right)\left(\frac{\beta}{1-\beta} n_{\mathrm{pho}} + n_{\mathrm{gly}}\right)}. \tag{A7}$$

A ratio of Δf_F to Δf_C is given by

$$\frac{\Delta f_F}{\Delta f_C} = \frac{\left(\frac{\alpha}{1-\alpha} n_{\mathrm{gla}} + n_{\mathrm{air}}\right)\left(\frac{\alpha}{1-\alpha} n_{\mathrm{gla}} + n_{\mathrm{gly}}\right)}{\left(\frac{\beta}{1-\beta} n_{\mathrm{pho}} + n_{\mathrm{air}}\right)\left(\frac{\beta}{1-\beta} n_{\mathrm{pho}} + n_{\mathrm{gly}}\right)}. \tag{A8}$$

$\Delta f_F/\Delta f_C$ is a function of α and β since $n_{\mathrm{gla}} = 2.28$, $n_{\mathrm{pho}} = 1.65$, $n_{\mathrm{gly}} = 1.47$, and $n_{\mathrm{air}} = 1.0$ are constants.

The side views of Figs. 3(a) and 3(b) show that the near field of the common SRR is distributed over the glass substrate in the regions of the SRR arms and gap, but that of the floating SRR is distributed over the photoresist pattern only in the region of the SRR arms. This result reveals $\beta < \alpha$. Figure 10 presents the dependencies of $\Delta f_F/\Delta f_C$ on β at arbitrary $\alpha = 0.2$, 0.4, 0.6, and 0.8. The theoretical results in Fig. 10 reveal $\Delta f_F/\Delta f_C > 1$ at $\beta < \alpha$. $\Delta f_F/\Delta f_C > 1$ reveals that the floating SRR has a larger frequency shifting range than the common SRR after the air overlayers are replaced by the glycerol overlayers. In addition, the floating and common SRRs have the same difference between the refractive indices of air and glycerol. Therefore, the floating SRR has a larger refractive index sensitivity than the common SRR. This result verifies the experimental spectra of Figs. 2(a) and 2(b).

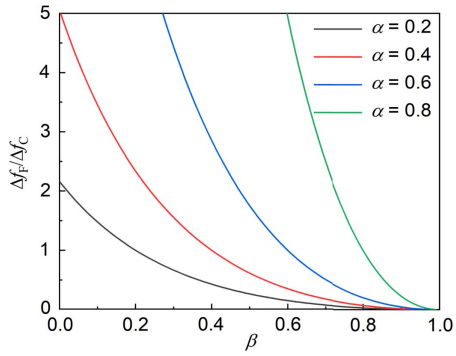

Fig. 10. Dependencies of $\Delta f_F/\Delta f_C$ on β at arbitrary $\alpha = 0.2$, 0.4, 0.6, and 0.8.

The SRRs in the floating metamaterial are lifted by the photoresist patterns with a terahertz refractive index of $n_{\mathrm{pho}} = 1.65$. In addition, Eq. (A7) reveals that Δf_F will be increased significantly as n_{pho} is decreased. It is interesting to study the frequency shifting range of a floating SRR using other lifting materials with terahertz refractive indices of n_{lif}. Therefore, n_{pho} in Eq. (A8) is replaced by n_{lif}.

Figure 11 presents the dependencies of $\Delta f_F/\Delta f_C$, which involves $n_{\mathrm{lif}} = 1.30$, 1.65, and 2.25 on β at $\alpha = 0.6$. The lifting materials are photopolymer, photoresist (SU-8 3010, Kayaku Advanced Materials (formerly MicroChem Corp.), Newton, MA, USA), and glass at $n_{\mathrm{lif}} = 1.30$, 1.65, and 2.25, respectively. The lifting material and substrate of the floating SRR compose an etched glass substrate at $n_{\mathrm{lif}} = 2.25$ because they are made of glass. The results in Fig. 11 reveal that the floating SRR has a smaller frequency shifting range at a given β as it is lifted by the etched glass substrate than by a photoresist pattern. Therefore, the etching of a substrate cannot increase the refractive index sensitivity of a terahertz metamaterial. The results in Fig. 11 reveal that the floating SRR has a larger frequency shifting range at a given β as it is lifted by a photopolymer pattern than by the photoresist pattern. If a photopolymer with a refractive index that is smaller than that of the photoresist used in this work, a floating terahertz metamaterial

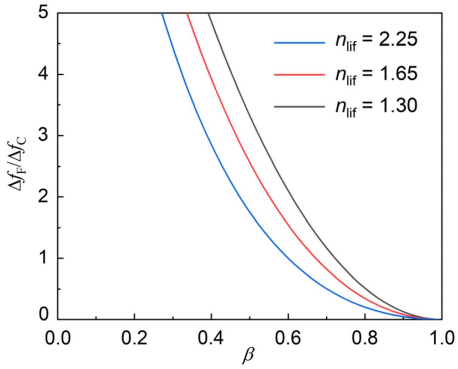

Fig. 11. Dependencies of $\Delta f_F/\Delta f_C$, which involve $n_{\mathrm{lif}} = 1.30$, 1.65, and 2.25, on β at $\alpha = 0.6$.

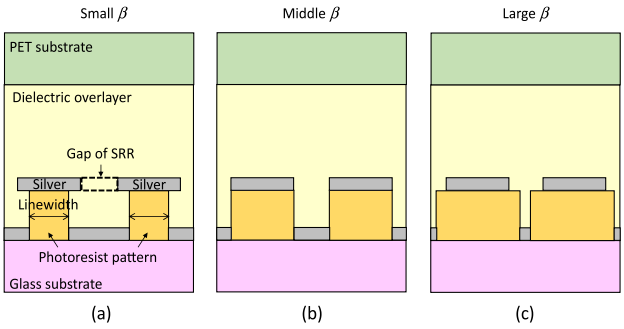

Fig. 12. Cases of (a) small, (b) middle, and (c) large β in design.

should have a refractive index sensitivity that exceeds 532 GHz/RIU.

Figure 12(a) presents the case of a small β that involves a floating SRR deposited on a photoresist pattern with a small linewidth. The floating SRR in this case has a small β because the dielectric region below the gap of the SRR is increased, and can be achieved by photolithography, thin film deposition, and wet etching. Figure 12(b) displays the case of a middle β that involves a floating SRR deposited on a photoresist pattern with a normal linewidth. Figure 12(c) presents the case of a large β that involves a floating SRR deposited on a photoresist pattern with a large linewidth. The floating SRR in this case has the large β because the dielectric region below the gap of the SRR is decreased, and can be achieved by photolithography and thin film deposition.

APPENDIX B: EFFECT OF COMPLEMENTARY SRR ON FLOATING SRR

The inset of Fig. 13(a) presents two floating SRRs. One comprises an SRR, photoresist pattern, and complementary SRR, and the other consists of an SRR and photoresist pattern. The photoresist patterns have an identical height of 30 μm in these floating SRRs. The one without a complementary SRR is used to study the effect of the complementary SRR on the electromagnetic resonance of the one with it. Figure 13(a) presents the simulated spectra of the floating SRRs with and without the complementary SRR at the air and glycerol overlayers. These floating SRRs have the same resonance frequency at 0.84 (0.59) THz as the air (glycerol) overlayers are deposited on them. This result reveals that the complementary SRR does not affect the resonance frequency of the floating SRR with it.

The inset of Fig. 13(b) displays a single complementary SRR. Figure 13(b) presents the simulated spectra of the single complementary SRR at the air and glycerol overlayers. The single complementary SRR has no resonance frequency at the air and glycerol overlayers. Therefore, the floating SRRs with and without the complementary SRR have the same resonance frequency at the air and glycerol overlayers. Because these floating SRRs have the same difference between the refractive indices of air and glycerol, they have the same refractive index sensitivity. The fabrication of a metamaterial that comprises floating SRRs with complementary SRRs is easier than that of a metamaterial that comprises floating SRRs without them because the fabrication of the latter requires two photolithography processes and an etching process. Therefore, the floating metamaterials with the complementary SRRs are used in this work.

Figure 13(b) displays that the single complementary SRR reduces the transmitted intensities of incident waves at terahertz frequencies as the air and glycerol overlayers are deposited on it. This result reveals that the complementary SRR in the floating SRR with it functions as a reflector. Therefore, the floating SRR with the complementary SRR has smaller transmittances at terahertz frequencies than that without a complementary SRR as the air and glycerol overlayers are deposited on them [Fig. 13(a)]. Current terahertz spectrometers can measure terahertz devices with small transmittances because they have large SNRs. Therefore, the method to increase the refractive index sensitivities of terahertz metamaterials using floating terahertz metamaterials with complementary SRRs is feasible. The floating SRR without its complementary SRR has a higher performance than that with its complementary SRR in terms of Q value and transmittance. Efforts are being made at the authors' laboratory to fabricate floating metamaterials without their complementary metamaterials, and the results will be published in the near future.

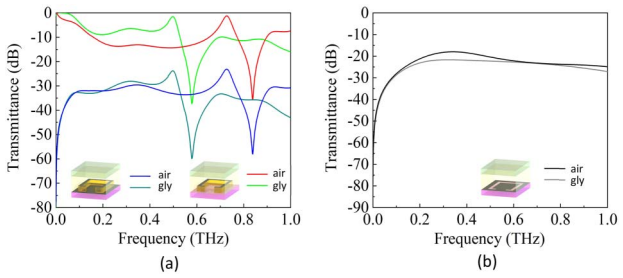

Fig. 13. (a) Simulated spectra of floating SRRs with and without complementary SRR at air and glycerol overlayers. (b) Simulated spectra of single complementary SRR at air and glycerol overlayers.

APPENDIX C: FLOATING METAMATERIAL ABSORBERS

Floating metamaterials can be used to develop terahertz absorbers. Figure 14(a) presents the schematic drawing of a terahertz absorber that involves a floating SRR. The terahertz absorber comprises a PET substrate, photoresist pattern, SRR, fluid

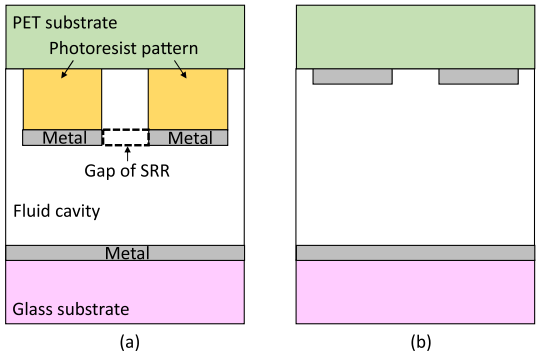

Fig. 14. Schematic drawing of terahertz absorbers that involve (a) floating and (b) common SRRs.

cavity, metal film, and glass substrate. Figure 14(b) presents the schematic drawing of a terahertz absorber that involves a common SRR. The terahertz absorber comprises a PET substrate, SRR, fluid cavity, metal film, and glass substrate. If the thickness of the photoresist pattern is large enough, the near field of the SRR will be far away from the PET substrate and will go deep into the fluid material in the cavity. The terahertz absorber that involves the floating SRR should have a larger refractive index sensitivity than the terahertz absorber that involves the common SRR because the near field of the floating SRR significantly interacts with the fluid material. Efforts are being made at the authors' laboratory to fabricate terahertz absorbers that involve floating metamaterials, and the results will be published in the near future.

Funding. Ministry of Science and Technology, Taiwan, China (MOST 110-2112-M-029-005).

Disclosures. The authors declare no conflicts of interest.

Data Availability. Data underlying the results presented in this paper are not publicly available at this time but may be obtained from the authors upon reasonable request.

REFERENCES

1. I. A. I. Al-Naib, C. Jansen, and M. Koch, "Thin-film sensing with planar asymmetric metamaterial resonators," Appl. Phys. Lett. **93**, 083507 (2008).
2. C. Sabah and H. G. Roskos, "Terahertz sensing application by using planar split-ring-resonator structures," Microsyst. Technol. **18**, 2071–2076 (2012).
3. W. F. Chiang, H. M. Silalahi, Y. M. Liu, Y. S. Lin, T. H. Chang, C. R. Lee, and C. Y. Huang, "Swelling of polydimethylsiloxane in toluene solutions on electromagnetic resonance of metamaterials," Appl. Phys. Lett. **115**, 211901 (2019).
4. W. J. Padilla, A. J. Taylor, C. Highstrete, M. Lee, and R. D. Averitt, "Dynamical electric and magnetic metamaterial response at terahertz frequencies," Phys. Rev. Lett. **96**, 107401 (2006).
5. D. J. Park, S. J. Park, I. Park, and Y. H. Ahn, "Dielectric substrate effect on the metamaterial resonances in terahertz frequency range," Curr. Appl. Phys. **14**, 570–574 (2014).
6. R. Cheng, L. Xu, X. Yu, L. Zou, Y. Shen, and X. Deng, "High-sensitivity biosensor for identification of protein based on terahertz Fano resonance metasurfaces," Opt. Commun. **473**, 125850 (2020).
7. Y. Li, X. Chen, F. Hu, D. Li, H. Teng, Q. Rong, W. Zhang, J. Han, and H. Liang, "Four resonators based high sensitive terahertz metamaterial biosensor used for measuring concentration of protein," J. Phys. D **52**, 095105 (2019).
8. K. Meng, S. J. Park, A. D. Burnett, T. Gill, C. D. Wood, M. Rosamond, L. H. Li, L. Chen, D. R. Bacon, J. R. Freeman, P. Dean, Y. H. Ahn, E. H. Linfield, A. G. Davies, and J. E. Cunningham, "Increasing the sensitivity of terahertz split ring resonator metamaterials for dielectric sensing by localized substrate etching," Opt. Express **27**, 23164–23172 (2019).
9. S. J. Park, J. T. Hong, S. J. Choi, H. S. Kim, W. K. Park, S. T. Han, J. Y. Park, S. Lee, D. S. Kim, and Y. H. Ahn, "Detection of microorganisms using terahertz metamaterials," Sci. Rep. **4**, 4988 (2014).
10. F. Taleb, I. Al-Naib, and M. Koch, "Free-standing complementary asymmetric metasurface for terahertz sensing applications," Sensors **20**, 2265 (2020).
11. S. Wang, L. Xia, H. Mao, X. Jiang, S. Yan, H. Wang, D. Wei, H. Cui, and C. Du, "Terahertz biosensing based on a polarization-insensitive metamaterial," IEEE Photon. Technol. Lett. **28**, 986–989 (2016).
12. X. Yan, M. Yang, Z. Zhang, L. Liang, D. Wei, M. Wang, M. Zhang, T. Wang, L. Liu, and J. Xie, "The terahertz electromagnetically induced transparency-like metamaterials for sensitive biosensors in the detection of cancer cells," Biosens. Bioelectron. **126**, 485–492 (2019).
13. A. S. Saadeldin, M. F. O. Hameed, E. M. A. Elkaramany, and S. S. A. Obayya, "Highly sensitive terahertz metamaterial sensor," IEEE Sens. J. **19**, 7993–7999 (2019).
14. J. H. Kang, J. H. Choe, D. S. Kim, and Q. H. Park, "Substrate effect on aperture resonances in a thin metal film," Opt. Express **17**, 15652–15658 (2009).
15. S. J. Park and Y. H. Ahn, "Substrate effects on terahertz metamaterial resonances for various metal thicknesses," J. Korean Phys. Soc. **65**, 1843–1847 (2014).
16. X. Hu, G. Xu, L. Wen, H. Wang, Y. Zhao, Y. Zhang, D. R. S. Cumming, and Q. Chen, "Metamaterial absorber integrated microfluidic terahertz sensors," Laser Photon. Rev. **10**, 962–969 (2016).
17. F. Yan, L. Li, R. Wang, H. Tian, J. Liu, J. Liu, F. Tian, and J. Zhang, "Ultrasensitive tunable terahertz sensor with graphene plasmonic grating," J. Lightwave Technol. **37**, 1103–1112 (2019).
18. L. Liang, X. Hu, L. Wen, Y. Zhu, X. Yang, J. Zhou, Y. Zhang, I. E. Carranza, J. Grant, C. Jiang, D. R. S. Cumming, B. Li, and Q. Chen, "Unity integration of grating slot waveguide and microfluid for terahertz sensing," Laser Photon. Rev. **12**, 1800078 (2018).
19. F. Lan, F. Luo, P. Mazumder, Z. Yang, L. Meng, Z. Bao, J. Zhou, Y. Zhang, S. Liang, Z. Shi, A. R. Khan, Z. Zhang, L. Wang, J. Yin, and H. Zeng, "Dual-band refractometric terahertz biosensing with intense wave-matter-overlap microfluidic channel," Biomed. Opt. Express **10**, 3789–3799 (2019).
20. M. Naftaly and R. E. Miles, "Terahertz time-domain spectroscopy of silicate glasses and the relationship to material properties," J. Appl. Phys. **102**, 043517 (2007).
21. Y. S. Jin, G. J. Kim, and S. G. Jeon, "Terahertz dielectric properties of polymers," J. Korean Phys. Soc. **43**, 513–517 (2006).
22. S. Arscott, F. Garet, P. Mounaix, L. Duvillaret, J.-L. Coutaz, and D. Lippens, "Terahertz time-domain spectroscopy of films fabricated from SU-8," Electron. Lett. **35**, 243–244 (1999).
23. R. P. Pan, C. F. Hsieh, C. L. Pan, and C. Y. Chen, "Temperature-dependent optical constants and birefringence of nematic liquid crystal 5CB in the terahertz frequency range," J. Appl. Phys. **103**, 093523 (2008).